PJET, Vol. 3, No. 1, October 2024: 1-17
Poly Journal of Engineering and Technology
journal homepage : https://journals.bdu.edu.et/index.php/PJET/index
ORIGINAL ARTICLE

# Transforming Water Hyacinth Biomass to Phosphate Absorbent Biochar with Mg/Al Layered Double Hydroxides

Yuka Takeshita[1], Shinjiro Sato[1*]

[1] Graduate School of Science and Engineering, Soka University, 1-236 Tangi-cho, Hachioji-shi, Tokyo, 192-8577, Japan

## Highlights:

- $PO_4^{3-}$-P adsorption process of BC-LDH was best described by the pseudo-second-order kinetic model.
- The Langmuir maximum $PO_4^{3-}$-P adsorption capacity was 45.7 mg $g^{-1}$ for BC-LDH.
- Electrostatic attraction, replacement of surface hydroxyl groups and porous structure of biochar by phosphate were mainly responsible for phosphate adsorption by BC-LDH.

**ABSTRACT**

In Lake Tana, Ethiopia, influx of nutrients has resulted in excessive growth of water hyacinth (WH) in the last decades, which has also caused economic and environmental problems. Although enormous labor and financial resources used to control this overgrowth, these were still not enough to suppress the excessive growth of WH. However, various studies have been conducted to effectively utilize biomass, with the view that such waste materials could potentially be utilized in a sustainable and low-cost manner. One of the effective uses of waste biomass is biochar, which is a pyrolyzed biomass under oxygen-limited conditions. Biochar has attracted much attention for its use as an adsorbent because of abundant functional groups on its surface and the porous structure. Recent research has been conducted to improve adsorption performance of biochar for anionic contaminants by applying metal modification to the biochar. In fact, it is reported that biochar-based layered double hydroxide (LDH) composite materials showed improved properties for removing phosphate ($PO_4^{3-}$). However, the performance of LDH-biochar as an adsorbent depends on the type of raw material used. Therefore, it is necessary to investigate $PO_4^{3-}$ adsorption properties of biochar derived from WH. Thus, the objective of this study was to determine $PO_4^{3-}$ adsorption capacity of biochar derived from WH modified with Mg/Al-LDH and investigate the adsorption mechanism. The Langmuir maximum $PO_4^{3-}$ adsorption capacity was 45.7 mg $g^{-1}$. The adsorption mechanism was mainly chemical monolayer adsorption, replacement of surface hydroxyl groups with $PO_4^{3-}$, the electrostatic attraction between LDH and $PO_4^{3-}$, and the porous structure of the biochar. In this study, LDH treatment was shown to be effective to improve $PO_4^{3-}$ adsorption capacity of biochar, however the adsorption capacity of Mg/Al-LDH biochar derived from WH was lower than other studies, suggesting that further research is needed.

***Keywords:*** *Keywords: biochar, layered double hydroxides, phosphorus, adsorption, water hyacinth*

*https://doi.org/10.20372/pjet.v3i1.1807*

***Corresponding Author:*** Shinjiro Sato
Graduate School of Science and Engineering, Soka University, 1-236 Tangi-cho, Hachioji-shi, Tokyo, 192-8577, Japan
*Email ssato@soka.ac.jp*

## 1. Introduction

Located in northwestern Ethiopia, Lake Tana is the largest freshwater lake in Ethiopia with an area of approximately 3050 $km^2$ and a basin area of approximately 16,500 $km^2$ (Dejen et al., 2017). In Lake Tana, water hyacinth (WH, *Eichhornia crassipes*) began to expand from 2011 due to high nutrients inflow from agricultural runoff and inadequate wastewater treatment and has covered about 40 km of the lake shore in less than 2 years (Worku & Sahile, 2017; Dejen et al., 2017). WH is known to be one of the most invasive plants in the world and is reported to grow to about twice its size only five days (Malik, 2007). Overgrowth of WH can reduce biodiversity by competitively eliminating submerged and floating plants (Hashem et al., 2020) and covering the water surface (Bote et al., 2020). In Ethiopia, the overgrowth of WH has caused not only environmental problems, but also socioeconomic problems such as the disruption of crop harvests and fishing activities (Enyew et al., 2020). To date, nearly 800,000 people have been involved in manual harvesting from 2012–2018 to control overgrown WH and more than one million US dollars has been spent on weeding machine and herbicides (Enyew et al., 2020). Yet, it is still not enough to keep up with the control of overgrowth of WH. Therefore, there is an urgent need to develop effective treatment and utilization methods for WH. There are many applications of WH are available such as bioenergy, adsorbent, and fertilizers. Among these, adsorbent is a potential application because of its porous structure (Nandiyanto et al., 2023).

In addition, global population growth and increase for food demand (Cooper et al., 2011; Van Vuuren et al., 2010) have resulted in large demands for phosphorus (P) fertilizer for agriculture (Alagha et al., 2020). Phosphorus is extracted from a non-renewable resource, phosphate rocks (Brunner. 2010), and since once released into the environment it is difficult to recover, it is considered a non-renewable resource (Cordell & White, 2011). In recent years, technologies to recover and recycle P have been conducted such as chemical precipitation, reverse osmosis, and adsorption (Lee et al., 2019; Mustafa et al., 2006). Among these, adsorption is considered a preferred technology because of its easy operation, low cost, and zero or minimal generation of harmful byproducts during operation (Lee et al., 2019).

Different types of adsorbents have been developed, including activated carbon, industrial solid waste, and biochar (Lee et al., 2019). Among these methods, biochar (BC) derived from agricultural waste and produced through pyrolysis of biomass under an oxygen-limited environment is considered a preferred method because of its porous structure, high specific surface area, ion exchange capacity, and environmentally friendliness (Li et al., 2016;). However, binding affinity of BC toward anionic contaminants is hindered because of negatively charged surface of BC. Therefore, recent researches have been conducted to improve adsorption performance for negatively charged ions of BC by metal modification to biochar.

Recently, biochar-based layered double hydroxides (LDH) have been attracted due to their favorable properties for its anion exchange properties, high specific surface area, and low cost. LDH is a type of multifunctional anionic clay synthesized with brucite-type host layers of positively charged divalent and trivalent metal oxides and negatively charged interlayer regions (Lee et al., 2019). The general formula of LDH is $[M^{2}_{1-x} + M^{3+}_{x} (OH)][A^{n-}]x/n \cdot yH_2O$, where $M^{2+}$ is the divalent metal ion ($Mg^{2+}$, $Zn^{2+}$, $Mn^{2+}$, $Co^{2+}$, $Ni^{2+}$, $Cd^{2+}$, etc.); $M^{3+}$ is the trivalent metal ion ($Al^{3+}$, $Fe^{3+}$, $Cr^{3+}$, $Ga^{3+}$, etc); and $A^{n-}$ is an anion ($PO_4^{3-}$, $CO_3^{2-}$, $NO_3^{-}$, $Cl^{-}$, etc.) that is incorporated into the interlayer to

neutralize the charge and to provide structural stability. LDH is composed of hydroxide layers, where the partial substitution of trivalent metal ions for divalent metal ions creates a positive charge in the interlayer and anions are incorporated into the layer (Xing et al., 2014). However, the adsorption capacity of LDH biochars depends on feedstock.

Therefore, the objective of this study was to determine phosphate ($PO_4^{3-}$) adsorption capacity of BC derived from WH modified with Mg/Al-LDH (BC-LDH) and investigate the adsorption mechanism.

## 2. Materials and Methods

### 2.1 Collection and preparation of biochar

Analytical grade aluminum chloride hexahydrate ($AlCl_3 \cdot 6H_2O$), magnesium chloride hexahydrate ($MgCl_2 \cdot 6H_2O$), sodium hydroxide (NaOH), hydrochloric acid (HCl), potassium dihydrogen phosphate ($KH_2PO_4$), and other reagents used for adsorbent synthesis and analysis were purchased from Wako Pure Chemical Industries, Ltd., Osaka, Japan.

WH sample used in this study was harvested from rice paddies in Kazo City, Saitama Prefecture, Japan in December 2020. Prior to use, WH was washed with deionized water followed by oven-drying at 105°C for 24 h. The dried WH was then ground, passed through a 1–2 mm sieve, and kept in a sealed container.

### 2.2 Modification of biochar with LDH

For BC modified with LDH production, WH was pyrolyzed in a steel container placed in an electric muffle furnace (FUW242PA, ADVANTEC) with a heating rate of 5°C $min^{-1}$ under limited oxygen supply, and 2 h of retention time at the highest heating temperature at 600°C. After pyrolysis, BC was dried in the oven at 105°C for 24 h, followed by sieving by a mesh with a pore diameter of <500 μm and stored in the dryer at 45°C before uses. BC (1.67 g) was mixed into 25 mL of aqueous solution containing 1.0 mol/L of $MgCl_2 \cdot 6H_2O$ and 1.0 mol/L of $AlCl_3 \cdot 6H_2O$. The pH of the mixtures was adjusted to 10 using 1.0 mol/L NaOH aqueous solution. The prepared black slurry (biochar with aqueous solution) was sealed in a bottle and incubated for 3 days at 80°C. The obtained BC-LDH composites were then dried at 105°C for 24 h, followed by sieving by a mesh with a pore diameter of <500 μm and stored in the dryer at 45°C before uses. BC without LDH treatment and pure-LDH without BC were also used for further experiments. The biochar adsorption amount of $PO_4^{3-}$-P was calculated by the equation (1).

$$q_e = \frac{(C_0 - C_e)V}{M} \quad (1)$$

where *qe* (mg g–1) is the amount of P adsorbed by biochar; *C0* (mg L–1) and *Ce* (mg L–1) are the

initial and equilibrium P concentration, respectively; *V* (L) is the volume of solution; and *M* (g) is the mass of biochar.

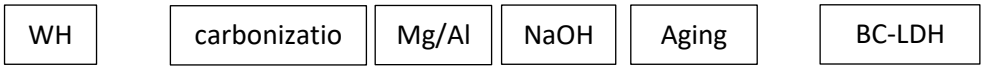

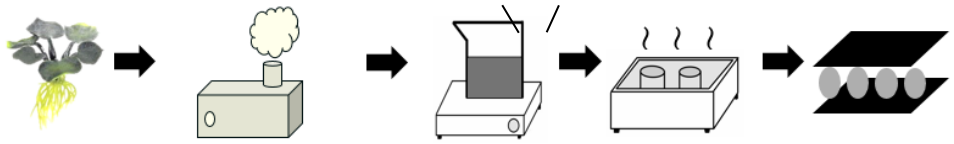

## 2.3 Batch adsorption experiments

### 2.3.1 Adsorption kinetics

To assess the effects of contact time, adsorption kinetic studies were carried out where the samples (BC, pure-LDH, and BC-LDH) were shaken at different interval times (15, 30, 60, 120, 240, 480, 720, and 1440 min). The initial $PO_4^{3-}$-P solutions pH were adjusted to 100 mg P $L^{-1}$ and 7.00 ± 0.05 (adjusted by 0.1 mol $L^{-1}$ of HCl or NaOH), respectively. The concentrations of $PO_4^{3-}$-P adsorbed onto each sample were calculated by Equation (2,3). Equation 2 is pseudo-first-order linear fitting and equation 3 is pseudo-second-order linear fitting. The experimental results were fitted with the pseudo-second-order model by Equation (2).

$$q_t = q_e(1 - e^{-k_1 t}) \quad (2)$$

$$q_t = \frac{k_1 q_e^2 t}{1 + k_1 q_e t} \quad (3)$$

where $q_e$ and $q_t$ (mg $g^{-1}$) refer to the adsorption amount at equilibrium and the adsorption amount homologous to the reaction time $t$ (min) of $PO_4^{3-}$-P; $k_1$ (g $mg^{-1}$ $min^{-1}$) is the rate constants of the models.

### 2.3.2 Effect of pH on phosphate adsorption

The effect of different pH of the initial $PO_4^{3-}$-P solution on adsorption was investigated with different four pH levels (2.0, 4.0, 6.0, and 8.0 ± 0.05 adjusted by 0.1 mol $L^{-1}$ of HCl or NaOH). The initial $PO_4^{3-}$-P concentration and contact time were 100 mg $L^{-1}$ and 480 min (determined in Section 2.2.1), respectively. The pH of the filtrate (i.e., equilibrium pH) was measured after every $PO_4^{3-}$-P adsorption experiment and the concentration of $PO_4^{3-}$-P were calculated by Equation (1).

### 2.3.3 Adsorption isotherm

To assess the effect of the initial $PO_4^{3-}$-P concentration on adsorption, different $PO_4^{3-}$-P concentrations were used (10, 20, 40, 80, 100, 150, 200, 300, 500, and 1000 mg P $L^{-1}$). The initial $PO_4^{3-}$-P solution pH and contact time were 6.0 ± 0.05 (determined in Section 2.2.2) and 480 min (determined in Section 2.2.1), respectively. The concentration of $PO_4^{3-}$-P adsorbed onto BC were calculated by Equation (1). Langmuir adsorption isotherm model by Equations 3 and Freundlich model by Equation 4 were used to check whether the experimental results fitted to either of these models.

$$q_e = \frac{C_e q_m K_L}{1 + C_e K_L} \quad (4)$$

$$q_e = K_F C_e^{1/n} \quad (5)$$

where $q_e$ (mg $g^{-1}$) and $C_e$ (mg $L^{-1}$) refer to the adsorption amount of $PO_4^{3-}$-P in equilibrium and the concentration of $PO_4^{3-}$-P in solution, respectively; $q_m$ (mg $g^{-1}$) represents the maximum adsorption amount of $PO_4^{3-}$-P by different

adsorbents; $K_L$ is the adsorption affinity constant; $K_F$ stands for Freundlich constant; *1/n* is non-linear constant.

### 2.4 Biochar characterization

The pH point of zero charge ($pH_{PZC}$) of BC, pure-LDH, and BC-LDH were determined according to pH drift method (Divband Hafshejani et al., 2016). After drying the samples at 105°C for 24 h, the surface morphology was observed using Scanning Electron Microscopy (JSM-5600LV, JEOL). BC-LDH samples before and after $PO_4^{3-}$ adsorption was measured for Fourier Transform Infra-Red spectroscopy (FTIR) analysis. BC-LDH after $PO_4^{3-}$ adsorption sample was filtered by filter paper (Whatman No. 1) and dried in an oven together with the filter paper at 105°C for 24 h. The adsorbed $PO_4^{3-}$-P amount by BC-LDH was confirmed by analyzing the remaining $PO_4^{3-}$-P in the filtrates and were equivalent to that by BC-LDH used for adsorption isotherm experiment. Sample surface functional groups were analyzed by FTIR after mixing 1.0 mg of sample with spectral-grade 100 mg potassium bromide (KBr) and ground in an agate mortar. The mixture was then compressed at about 7845 kPa for 2 min into a 13 mm sample pellet. A background spectrum was obtained each time before the samples were processed. All spectra between 4000 and 400 $cm^{-1}$ was collected at a spectral resolution of 2 $cm^{-1}$ and 64 scans. Spectral analysis was performed using Omnic 9 software (Thermo Scientific).

### 2.4 Statistical analyses

Statistical analyses were carried out using the statistical software Statistica 6.1 (StatSoft. Inc., Tulsa, OK, USA). Treatment effects were analyzed by one-way analysis of variance (ANOVA). A Tukey honestly significant difference (HSD) analysis was performed for multiple comparisons of the treatment effects (n = 3). Statistical significances were determined at $P < 0.05$.

## 3. Results and Discussion

### 3.1 Batch phosphate adsorption

### 3.1.1 Optimization of the initial solution pH for adsorption

The $PO_4^{3-}$-P adsorption increased with increasing pH from 2 to 6, with the maximum adsorption of 13.5 mg $g^{-1}$ at pH 6 (Fig. 1). The adsorption amounts decreased with further increasing pH to 12 (2.15–7.48 mg $g^{-1}$). This could be attributed to different P species at different solution pH. Among the four phosphate chemical forms ($H_3PO_4$, $H_2PO_4^-$, $HPO_4^{2-}$, and $PO_4^{3-}$), $H_2PO_4^-$ and $HPO_4^{2-}$ are the dominant species in the studied pH range of 3–7 and 7–9, respectively (Chubar et al., 2005). Since the adsorption free energy of $H_2PO_4^-$ was lower than that of $HPO_4^{2-}$ (Chowdhury and Yanful, 2010; Chubar et al., 2005), $H_2PO_4^-$ is more easily adsorbed by adsorbents than $HPO_4^{2-}$. Moreover, the adsorption amount decreased under acidic conditions below pH 6. This can be attributed to the significant metal-metal-hydroxy-salts (Mg/Al-LDH) dissolution at acidic conditions which adversely affected phosphate uptake (Yang et al. 2019). In this study, the adsorption amounts also decreased under basic condition above pH 6. This may be because of the competition between $PO_4^{3-}$ and $OH^-$ for the adsorption sites of BC-LDH under basic condition (Hatami et al., 2018). Thus, pH 6 was the optimum initial solution pH for $PO_4^{3-}$-P adsorption because there were few presences of ions that inhibited adsorption.

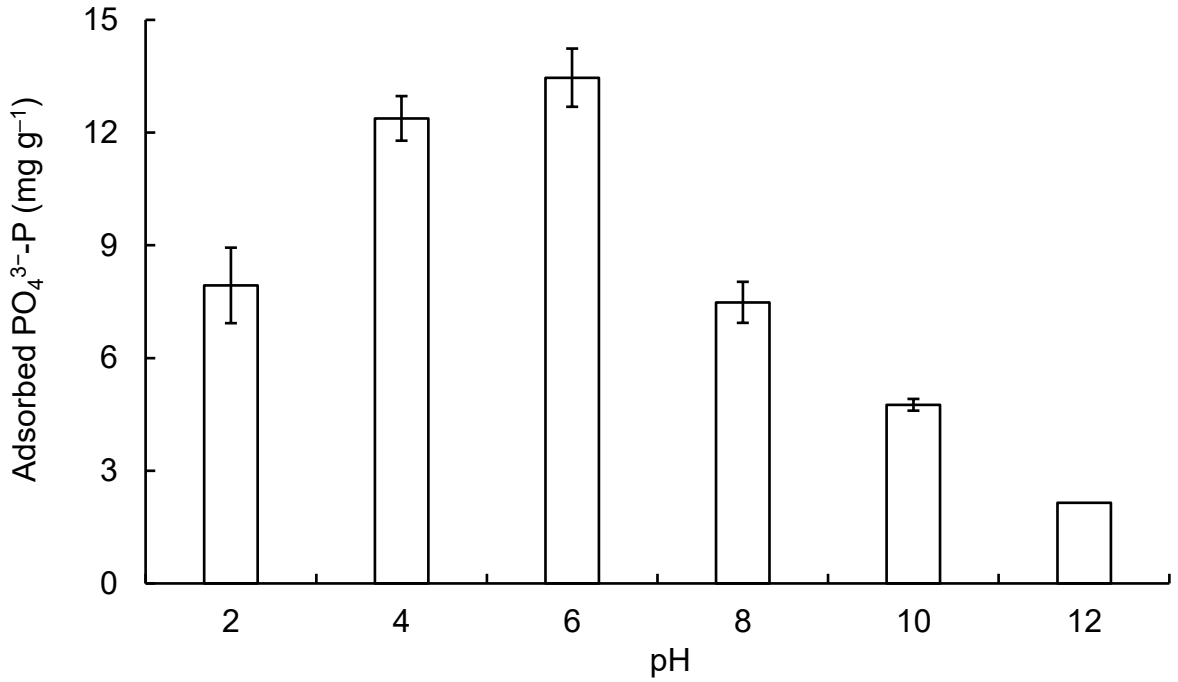


Figure 1. Effect of different initial solution pH for phosphate adsorption on BC-LDH. Vertical bars represent standard deviations (n = 3).

### 3.1.2 Adsorption kinetics

The $PO_4^{3-}$-P adsorption of BC-LDH reached an equilibrium at around 480 min, with the maximum adsorption amount of 11.7 mg $g^{-1}$ (Fig. 2b). The pseudo-second-order model fitted well to kinetic data ($R^2$ = 0.999 Fig. 2b). The pseudo-second-order model represents a chemisorption mechanism (Zheng et al., 2020). This suggests that chemisorption could be the predominant adsorption mechanism for BC-LDH. Chemisorption is included mainly by ion exchange, covalent ions, precipitation, complex formation, and chemical reactions with functional groups (Takaya et al., 2016). The maximum adsorption calculated from the pseudo-second-order model (qe = 11.8 mg $g^{-1}$) and the measured maximum adsorption when equilibrium was reached (qt = 11.5 mg $g^{-1}$) were also very close. The initial rapid adsorption may be believed to be due to electrostatic attraction between the positively charged metal oxide and the negatively charged phosphate ions and subsequent slow adsorption involves intraparticle diffusion (Li et al., 2016).

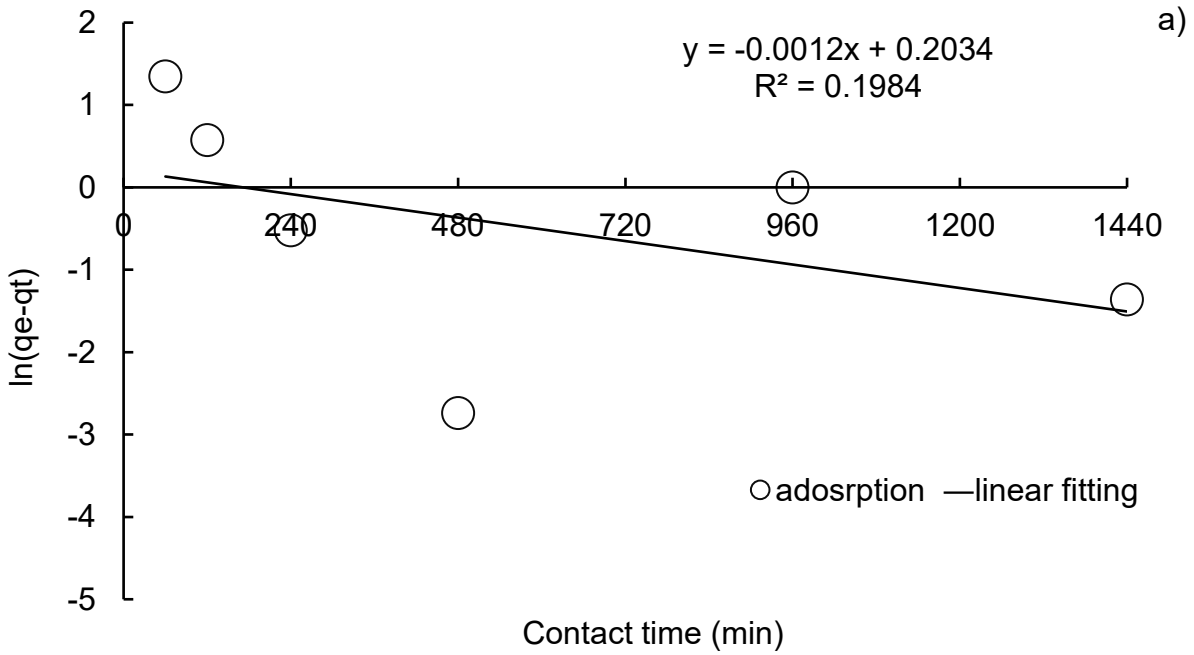
a)
y = -0.0012x + 0.2034
R² = 0.1984
2
1
0
-1
-2
-3
-4
-5
0
240
480
720
960
1200
1440
ln(qe-qt)
adosrption —linear fitting
Contact time (min)

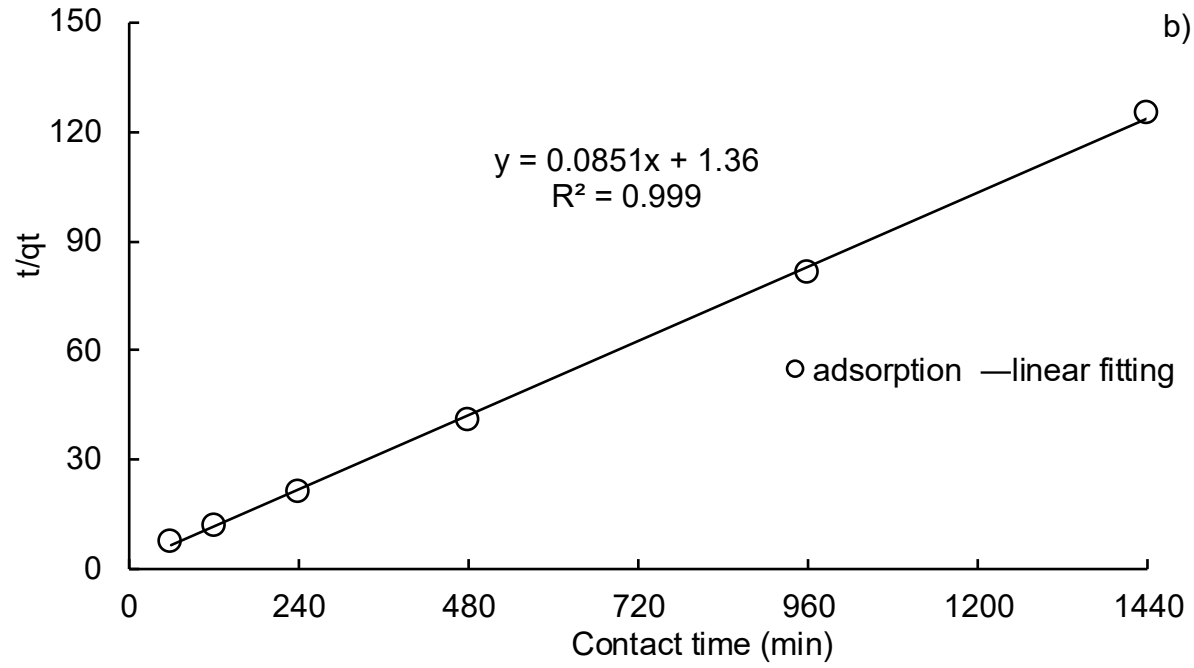
b)
y = 0.0851x + 1.36
R² = 0.999
150
120
90
60
30
0
0
240
480
720
960
1200
1440
t/qt
adsorption —linear fitting
Contact time (min)

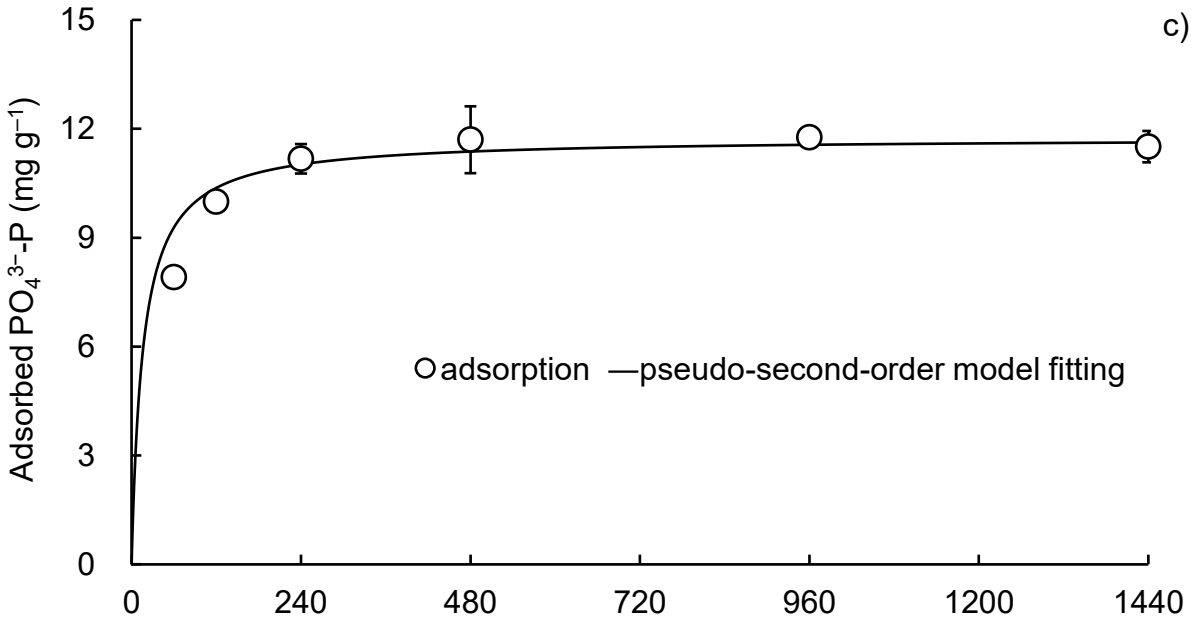


Figure 2. Adsorption kinetics of phosphate on BC-LDH with a) pseudo-first-order linear fitting, b) pseudo-second-order linear fitting, and c) pseudo-second-order model fitting of experimental data plot. Vertical bars represent standard deviations (n = 3).

### 3.1.3 Adsorption isotherm

The adsorption isotherms showed different behaviors for different adsorbents, and Langmuir model fitted well to all adsorption isotherms (Fig. 3). The Langmuir maximum $PO_4^{3-}$-P adsorption capacity (qm) was 15.8, 23.2, and 45.7 mg $g^{-1}$ for BC, pure-LDH, and BC-LDH, respectively (Table 1). The maximum adsorption capacity of BC-LDH was about 3-times and about twice higher than those of BC and pure-LDH, respectively.

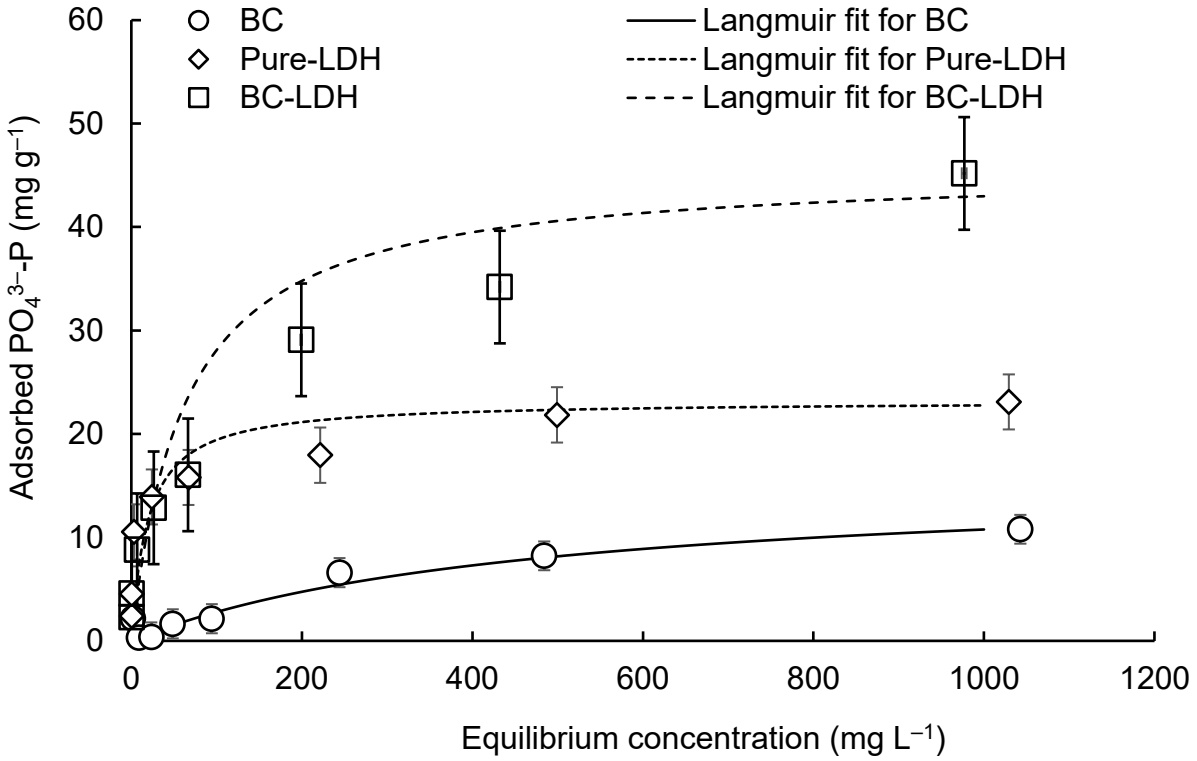


Figure 3. Adsorption isotherms of phosphate on adsorbents with Langmuir model fit of experimental data plot. Vertical bars represent standard deviations (n = 3).

Table 1. Parameters of adsorption isotherm models for phosphate on different adsorbents

| Sample | Langmuir | | | Freundlich | | |
|---|---|---|---|---|---|---|
| | $K_L$ (mg $L^{-1}$) | qm (mg $g^{-1}$) | $R^2$ | n | $K_F$ (mg $g^{-1}$) | $R^2$ |
| BC | 0.00215 | 15.8 | 0.647 | 2.16 | 3.45 | 0.530 |
| Pure-LDH | 0.0514 | 23.2 | 0.996 | 4.06 | 2.15 | 0.881 |
| BC-LDH | 0.0160 | 45.7 | 0.972 | 2.92 | 1.18 | 0.967 |

BC: pristine biochar, Pure-LDH: pure LDH, BC-LDH: biochar modified with LDH

The Langmuir model defines adsorption as monolayer adsorption with a uniform adsorbent surface (Tan et al., 2016), whereas the Freundlich model defines multilayer adsorption on an adsorbent with a heterogeneous surface (Y. Yang et al., 2014). Pure-LDH and BC-LDH fitted the Langmuir model ($R^2$ = 0.996 and 0.972, respectively; Table 1; Fig. 4a) better than the Freundlich model ($R^2$ = 0.881 and 0.967, respectively; Table 1; Fig. 4b). This suggests that the

$PO_4^{3-}$-P adsorption of pure-LDH and BC-LDH were mainly due to chemotactic monolayer adsorption. On the other hand, BC did not fit well to both of Langmuir ($R^2 = 0.647$; Table 1; Fig. 4a) and Freundlich models ($R^2 = 0.530$; Table 1; Fig. 4b).

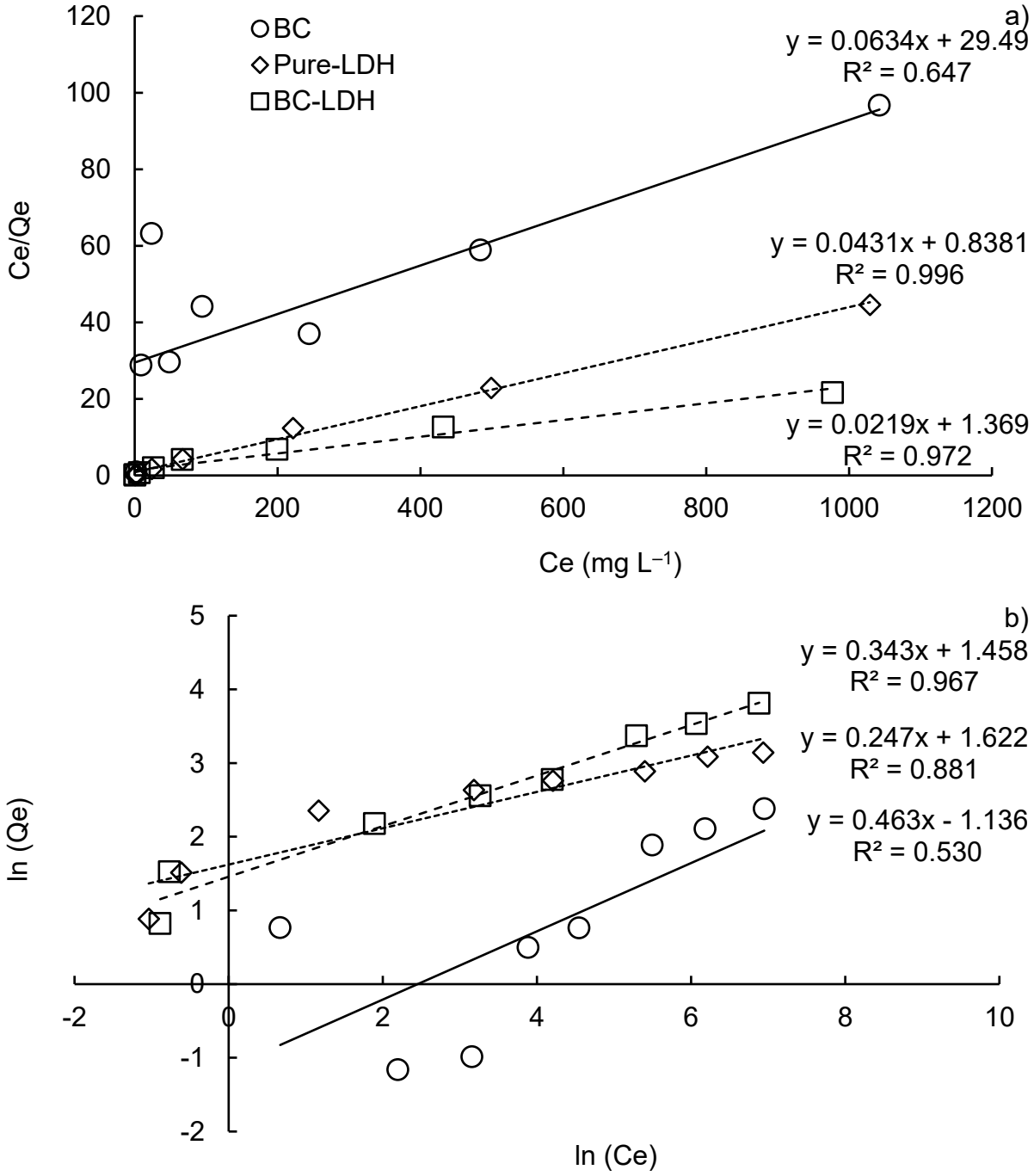


Figure 4. Linear fitting of adsorption isotherms of phosphate on adsorbents for a) Langmuir linear model and b) Freundlich linear model

### 3.2 Phosphate adsorption mechanism

The $pH_{PZC}$ of adsorbent indicates the pH at which the surface charge of adsorbent is apparently neutralized in aqueous solution to plus or minus zero. In other words, when the solution pH is lower than $pH_{PZC}$, the adsorbent surface is positively charged, while when the solution pH is higher than $pH_{PZC}$, the adsorbent surface is negatively charged (Chikazawa, 1993; Moirana et al., 2023). The $pH_{PZC}$ of pure-LDH and BC-LDH were 8.53 and 8.85, respectively (Fig. 5), indicating that pure-LDH and BC-LDH were positively charged when the solution pH was lower than 8.53 and 8.85, respectively. This suggests that at solution pH 6.0, adsorption between $PO_4^{3-}$-P and pure-LDH and BC-LDH occurred due to chemical and electrostatic attraction (Novillo et al., 2014). On the other hand, $pH_{PZC}$ of BC showed 5.18 which was lower than solution pH 6.0. Therefore, the surface charge of BC became negative, suggesting that the $PO_4^{3-}$-P adsorption decreased due to electrostatic repulsion.

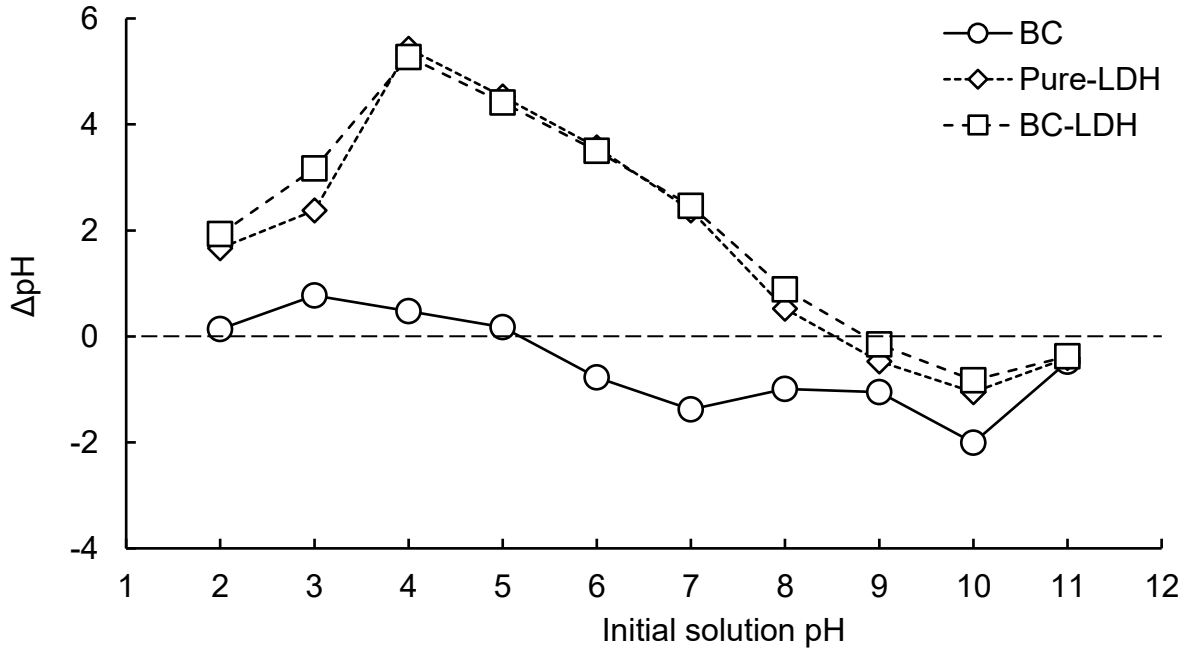


Figure 5. Equilibrium pH for effect of different initial solution pH for phosphate adsorption on biochars.

The results of SEM image after $PO_4^{3-}$-P adsorption for BC, pure-LDH, and BC-LDH are shown (Fig. 6). For BC, biochar porous structure was observed on the surface. This suggests that the $PO_4^{3-}$-P adsorption of BC was due mainly to pore filling of $PO_4^{3-}$-P ions. On the contrary, the surface of pure-LDH possessed a well-developed layered structure. For BC-LDH, both biochar porous and layered structure of LDH were observed, suggesting that the $PO_4^{3-}$-P adsorption of BC-LDH was due mainly to the pore filling of $PO_4^{3-}$-P ions and anion exchange reaction by LDH structure.

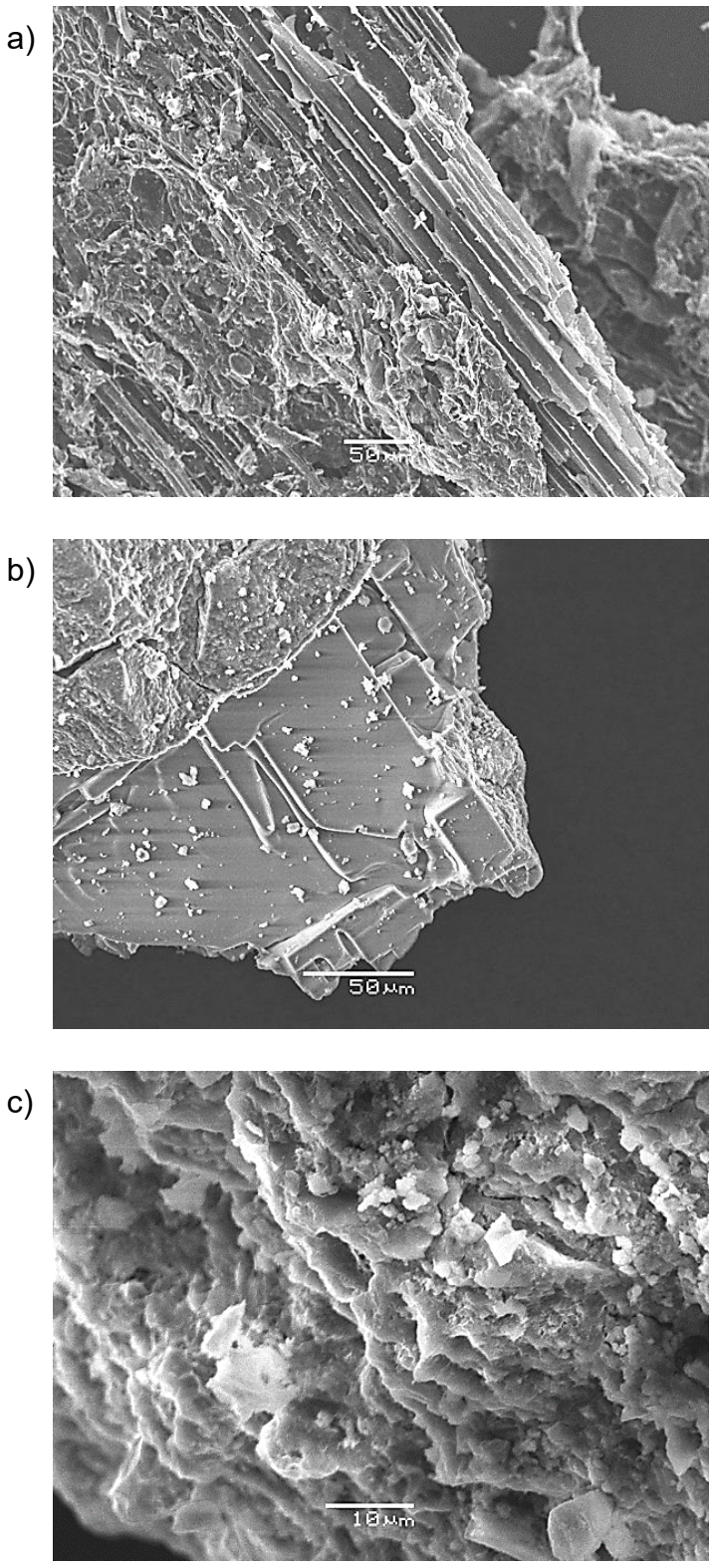


Figure 6. SEM images of a) BC, b) pure-LDH, and c) BC-LDH after phosphate adsorption

FTIR of BC-LDH before $PO_4^{3-}$-P adsorption showed that the peaks at 684, 779, and 881 $cm^{-1}$ seen below 1000 $cm^{-1}$ were attributed to the stretching vibrations of Mg–O or $Al_2O_3$ (Fig. 7a; Shabanian et al., 2020). The peak at 1363 $cm^{-1}$ is attributed to the stretching vibrations of intermediate layer carbonate species (Dai et al., 2023). The peak at 1618 $cm^{-1}$ is attributed to the stretching vibrations of C=C (Nanda et al., 2013). The peak at 2976 $cm^{-1}$ is associated with the O–H starching vibrations of interlayer water molecules (Abd-Ellatif et al., 2022). The broad band centered at 3471 $cm^{-1}$ are assigned to carboxylate-derived O–H in WH (Suthar et al., 2022) or to the O–H stretching vibrations of interlayer water molecules (Lee et al., 2019). FTIR of BC-LDH after $PO_4^{3-}$-P adsorption showed that the peaks at 779 and 673 $cm^{-1}$ after adsorption were reduced compared to those before adsorption (Fig. 7b). This suggests that Al–O and Mg–O could be involved in the $PO_4^{3-}$-P adsorption. The decrease or disappearance of the peaks below 1000 $cm^{-1}$ and the appearance of the peak at 1091 $cm^{-1}$ indicates that $PO_4^{3-}$-P was adsorbed possibly through the monodentate and bidentate inner-sphere surface complexes, suggesting that $PO_4^{3-}$-P was adsorbed on metal oxides (Mg–O and Al–O) through monodentate and bidentate inner-sphere complexes (Li et al., 2016). The peak at around 1091 $cm^{-1}$ is assigned to $HPO_4^{2-}$ and asymmetric stretching of P–O or targeted stretching of P–O (Shabanian et al., 2020). The decrease of the peak in O–H suggested that the hydroxyl groups were probably replaced during the adsorption of $PO_4^{3-}$-P and the observed corresponding increase in solution pH with $PO_4^{3-}$-P adsorption was consistent with ligand exchange with surface hydroxyls (Li et al., 2016). The results of FTIR using $NO_3^-$ as ions incorporated into the interlayer confirmed that ion exchange between $NO_3^-$ and $PO_4^{3-}$ ion has occurred (Li et al., 2016). However, in this study, since $Cl^-$did not have a significant and clear absorption band in the FTIR spectrum of LDH (Shabanian et al., 2020), it could not be confirmed whether ion exchange occurred or not.

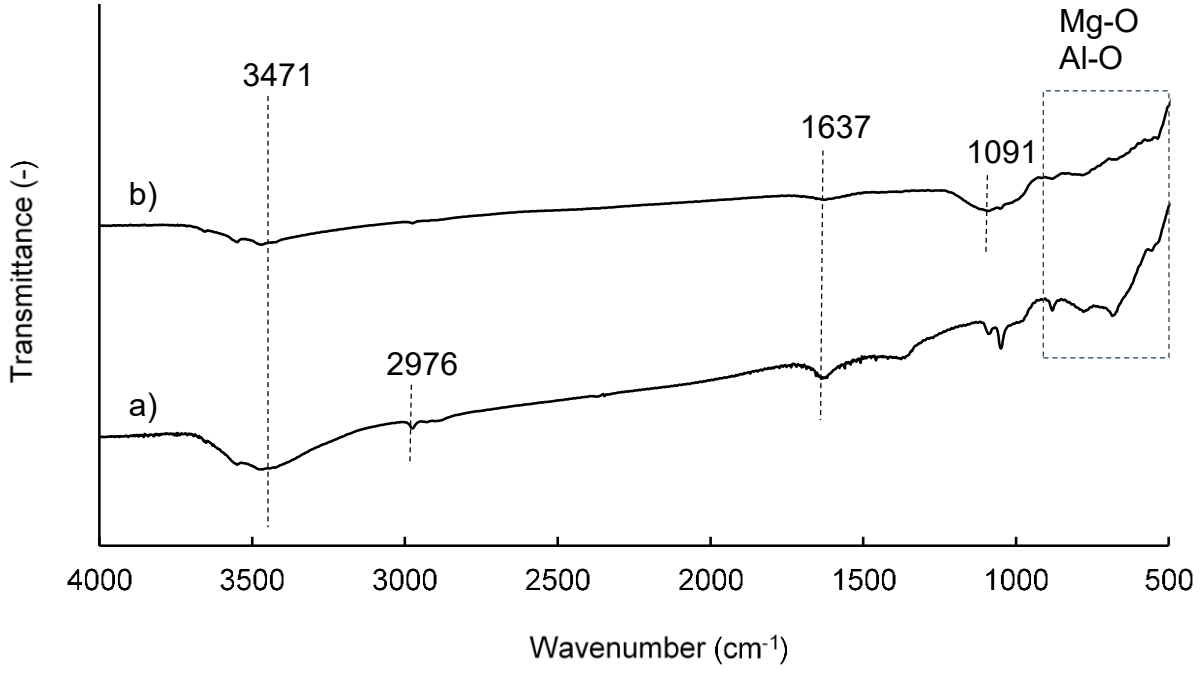


Figure 7. FTIR spectra of BC-LDH a) before and b) after adsorption of phosphate.
Dotted lines represent the detected spectral peaks in each biochar.

## 4. Conclusion

BC-LDH derived from WH showed insufficient adsorption capacity for practical use as an adsorbent. The $PO_4^{3-}$-P adsorption process of BC-LDH was best described by the pseudo-second-order kinetic model and reached equilibrium at 8 h. The Langmuir maximum $PO_4^{3-}$-P adsorption capacity was 15.8, 23.2, and 45.7 mg $g^{-1}$ for BC, pure-LDH, and BC-LDH, respectively. The results of this study indicated that electrostatic attraction, replacement of surface hydroxyl groups and porous structure of biochar by phosphate were mainly responsible for phosphate adsorption by BC-LDH. In this study, BC-LDH showed the highest adsorption performance compared to BC and pure-LDH, but the results were not enough to be practically used as an adsorbent. However, this study provided important insights into the mechanism of phosphate adsorption by biochar derived from WH modified with Mg/Al-LDH. In addition, using biochar adsorbent derived from water hyacinth as a low-cost and sustainable waste management method is expected to contribute to the effective use of waste biomass. Moreover, promoting biochar production by offering financial incentives or subsidies to companies leads to build a sustainable society.

## Author's contributions

Data curation: Yuka Takeshita. Investigation: Yuka Takeshita. Writing—original draft preparation: Yuka Takeshita. Writing—reviewing and editing: Shinjiro Sato. Project administration: Shinjiro Sato. Resources: Shinjiro Sato. Supervision: Shinjiro Sato.

## Funding

This study was partially supported by Japan Science and Technology Agency (JST)/Japan International Cooperation Agency (JICA), Science and Technology Research Partnership for Sustainable Development (SATREPS) through the project for Eco-Engineering for Agricultural Revitalization toward Improvement of Human Nutrition (EARTH): Water Hyacinth to Energy and Agricultural Crops (grant number: JPMJSA2005).

## Competing interests

The authors declare that they have no known competing financial interests or personal relationships that could have appeared to influence the work reported in this paper.

## References

Abd-Ellatif, W. R., Mahmoud, N. G., Hashem, A. A., El-Aiashy, M. K., Ezzo, E. M., & Mahmoud, S. A. (2022). Efficient photodegradation of E124 dye using two-dimensional Zn-Co LDH: Kinetic and thermodynamic studies. Environmental Technology & Innovation, 27, 102393. https://doi.org/10.1016/j.eti.2022.102393

Alagha, O., Manzar, M. S., Zubair, M., Anil, I., Mu'azu, N. D., & Qureshi, A. (2020). Comparative Adsorptive Removal of Phosphate and Nitrate from Wastewater Using Biochar-MgAl LDH Nanocomposites: Coexisting Anions Effect and Mechanistic Studies. Nanomaterials, 10(2), 336. https://doi.org/10.3390/nano10020336

Asep Bayu Dani Nandiyanto., Risti Ragadhita., Siti Nur Hoffah., Dwi Fitria Al Husaeni., Dwi Novia Al Husaeni., Meli Fiandini., Senny Luckiardi., Eddy Soeryanto Soegoto., Arif Darmawan., Muhammad Aziz4 (2023). Progress in the utilization of water hyacinth as efective biomass material. Environment, Development and Sustainability (2024) 26:24521–24568 https://doi.org/10.1007/s10668-023-03655-6

Bote, M. A., Naik, V. R., & Jagadeeshgouda, K. B. (2020). Review on WH weed as a potential bio fuel crop to meet collective energy needs. In Materials Science for Energy Technologies ( Vol. 3, pp. 397–406). KeAi Communications Co. https://doi.org/10.1016/j.mset.2020.02.003

Dai, X., Jing, C., Li, K., Zhang, X., Song, D., Feng, L., Liu, X., Ding, H., Ran, H., Zhu, K., Dai, N., Yi, S., Rao, J., & Zhang, Y. (2023). Enhanced bifunctional adsorption of anionic and cationic pollutants by MgAl LDH nanosheets modified montmorillonite via acid-salt activation. Applied Clay Science, 233, 106815. https://doi.org/10.1016/j.clay.2023.106815

Dejen, E., Anteneh, W., & Vijverberg, J. (2017). The Decline of the Lake Tana (Ethiopia) Fisheries: Causes and Possible Solutions. Land Degradation & Development, 28(6), 1842–1851. https://doi.org/10.1002/ldr.2730

Divband Hafshejani, L., Hooshmand, A., Naseri, A. A., Mohammadi, A. S., Abbasi, F., & Bhatnagar, A. (2016). Removal of nitrate from aqueous solution by modified sugarcane bagasse biochar. Ecological Engineering, 95, 101–111. https://doi.org/10.1016/j.ecoleng.2016.06.035

Enyew, B. G., Assefa, W. W., & Gezie, A. (2020). Socioeconomic effects of WH (Echhornia Cra ssipes) in Lake Tana, North Western Ethiopia. PLOS ONE, 15(9), e0237668. https://doi.org /10.1371/journal.pone.0237668

Hatami, H., Fotovat, A., & Halajnia, A. (2018). Comparison of adsorption and desorption of phos phate on synthesized Zn-Al LDH by two methods in a simulated soil solution. Applied Cla y Science, 152, 333–341. https://doi.org/10.1016/j.clay.2017.11.032

Lee, S. Y., Choi, J.-W., Song, K. G., Choi, K., Lee, Y. J., & Jung, K.-W. (2019). Adsorption and mechanistic study for phosphate removal by rice husk-derived biochar functionalized with Mg/Al-calcined layered double hydroxides via co-pyrolysis. Composites Part B: Engineerin g, 176, 107209. https://doi.org/10.1016/j.compositesb.2019.107209

Li, R., Wang, J. J., Zhou, B., Awasthi, M. K., Ali, A., Zhang, Z., Gaston, L. A., Lahori, A. H., & Mahar, A. (2016). Enhancing phosphate adsorption by Mg/Al layered double hydroxide fun ctionalized biochar with different Mg/Al ratios. Science of The Total Environment, 559, 12 1–129. https://doi.org/10.1016/j.scitotenv.2016.03.151

Nanda, S., Mohanty, P., Pant, K. K., Naik, S., Kozinski, J. A., & Dalai, A. K. (2013). Characteriz ation of North American Lignocellulosic Biomass and Biochars in Terms of their Candidac y for Alternate Renewable Fuels. BioEnergy Research, 6(2), 663–677. https://doi.org/10.10 07/s12155-012-9281-4

Novillo, C., Guaya, D., Allen-Perkins Avendaño, A., Armijos, C., Cortina, J. L., & Cota, I. (2014 ). Evaluation of phosphate removal capacity of Mg/Al layered double hydroxides from aqu eous solutions. Fuel, 138, 72–79. https://doi.org/10.1016/j.fuel.2014.07.010

Shabanian, M., Hajibeygi, M., & Raeisi, A. (2020). FTIR characterization of layered double hydr oxides and modified layered double hydroxides. In Layered Double Hydroxide Polymer Na nocomposites (pp. 77–101). Elsevier. https://doi.org/10.1016/B978-0-08-101903-0.00002-7

Suthar, S., Sharma, B., Kumar, K., Rajesh Banu, J., & Tyagi, V. K. (2022). Enhanced biogas pro duction in dilute acid-thermal pretreatment and cattle dung biochar mediated biomethanatio n of WH. Fuel, 307, 121897. https://doi.org/10.1016/j.fuel.2021.121897

Takaya, C. A., Fletcher, L. A., Singh, S., Anyikude, K. U., & Ross, A. B. (2016). Phosphate and ammonium sorption capacity of biochar and hydrochar from different wastes. Chemospher e, 145, 518–527. https://doi.org/10.1016/j.chemosphere.2015.11.052

Tan, X., Liu, Y., Gu, Y., Liu, S., Zeng, G., Cai, X., Hu, X., Wang, H., Liu, S., & Jiang, L. (2016). Biochar pyrolyzed from MgAl-layered double hydroxides pre-coated ramie biomass (Boeh meria nivea (L.) Gaud.): Characterization and application for crystal violet removal. Journa l of Environmental Management, 184, 85–93. https://doi.org/10.1016/j.jenvman.2016.08.07 0

Van Vuuren, D. P., Bouwman, A. F., & Beusen, A. H. W. (2010). Phosphorus demand for the 19 70–2100 period: A scenario analysis of resource depletion. Global Environmental Change, 20(3), 428–439. https://doi.org/10.1016/j.gloenvcha.2010.04.004

Worku, M., & Sahile, S. (2017). Impact of WH, Eichhornia crassipes (Martius) (Pontederiaceae) in Lake Tana Ethiopia: A Review. Journal of Aquaculture Research & Development, 09(01 ). https://doi.org/10.4172/2155-9546.1000520

Yang, F., Zhang, S., Sun, Y., Tsang, D. C. W., Cheng, K., & Ok, Y. S. (2019). Assembling bioch ar with various layered double hydroxides for enhancement of phosphorus recovery. Journ al of Hazardous Materials, 365, 665–673. https://doi.org/10.1016/j.jhazmat.2018.11.047